INSTITUTE OF PHYSICS PUBLISHING PHYSICS IN MEDICINE AND BIOLOGY

Phys. Med. Biol. **49** (2004) N155–N163 PII: S0031-9155(04)75972-2

NOTE

Diffuse optical tomography with physiological and spatial *a priori* constraints

Xavier Intes[1,2,4], Clemence Maloux[1], Murat Guven[3], Birzen Yazici[3] and Britton Chance[1]

[1] Department of Biophysics and Biochemistry, University of Pennsylvania, Philadelphia, PA 19104, USA
[2] Department of Physics and Astronomy, University of Pennsylvania, Philadelphia, PA 19104, USA
[3] Department of Electrical, Computer, and Systems Engineering, Rensselaer Polytechnic Institute, Troy, NY 12180, USA

E-mail: xintes@art.ca

Received 5 February 2004
Published 26 May 2004
Online at stacks.iop.org/PMB/49/N155
DOI: 10.1088/0031-9155/49/12/N01

Abstract

Diffuse optical tomography is a typical inverse problem plagued by ill-condition. To overcome this drawback, regularization or constraining techniques are incorporated in the inverse formulation. In this work, we investigate the enhancement in recovering functional parameters by using physiological and spatial *a priori* constraints. More accurate recovery of the two main functional parameters that are the blood volume and the relative saturation is demonstrated through simulations by using our method compared to actual techniques.

(Some figures in this article are in colour only in the electronic version)

1. Introduction

Probing human tissue with near infrared (NIR) light is emerging as a new, promising imaging modality. The strength of this new technology relies on its ability to reveal the functional state of deep tissue. To date the main applications of NIR technologies are functional brain imaging (Strangman *et al* 2002, Villringer and Chance 1997), muscle imaging (Lin *et al* 2002) and optical mammography (Colak *et al* 1999, Franceschini *et al* 1997, Grosenick *et al* 2003, Intes *et al* 2003, Jiang *et al* 2002, McBride *et al* 2001, Tromberg *et al* 2000). The last application is known to be of growing interest in both the research and medical community (Cerussi and Tromberg 2003).

Optical mammography aims to retrieve important, local physiological parameters that are the blood content and the relative oxygenation of the blood. These two functional

[4] Now with ART Advanced Research Technologies.

parameters are known to provide a means of discriminating between healthy and diseased tissues. The blood content relates to the angiogenesis level of the tumourous mass, and the relative oxygenation to its hypermetabolic state. These two functional signatures correlate to malignancy.

Pre-clinical data strengthen these assumptions. However, difficulties arise due to the specific nature of the light propagation. In this spectral window, the light is strongly diffused leading to a relatively poor resolution for thick tissue investigation. Also, the breast is by nature a heterogeneous organ with a complex spatial distribution of optical relevant chromophores. In the NIR spectral range, four chromophores are accountable for the absorption (Cerussi *et al* 2001). These chromophores are the oxy- ($[HbO_2]$), deoxy-haemoglobin ([Hb]), the water ($[H_2O]$) and the lipids ([Li]). The first two chromophores are providing an insight into the tissue functional state. The last two chromophores are linked to the structural architecture of the breast. The spatial distribution and the relative concentrations of these chromophores are patient dependent and even more can vary over time in the same patient due to hormonal regulation (Chance 2001, Cubeddu *et al* 2000, Durduran *et al* 2002, Shah *et al* 2001, Srinivasan *et al* 2003).

To enhance diffuse optical tomography (DOT) performances, researchers have proposed fusing optical techniques with other medical imaging modality. Magnetic resonance imaging (MRI) is the perfect candidate for optical co-registration (Brooksby *et al* 2003, Guven *et al* 2004, Ntziachristos *et al* 2002, Pei *et al* 1999, Pogue and Paulsen 1998). MRI provides high spatial resolution maps of the breast optical structure that are relevant to the water and lipid distribution. Moreover, MRI can provide a means to estimate the concentration of these two structural chromophores (Merrit *et al* 2003). In this paper, we investigate the first step towards incorporating physiological and spatial *a priori* information derived from MRI.

2. Methods

2.1. Forward model

The propagation of NIR light in tissue is well modelled by the diffusion equation. In the case of heterogeneity, the diffusion equation can be solved by a perturbative approach (O'Leary 1996). In this work, we have used the Rytov approximation approach. In the case of DOT, multiple source–detector pairs are used. The medium under consideration is sampled in voxels and the problem can be written as a matrix equation (Arridge 1999), i.e.:

$$\begin{pmatrix} \Phi(r_{s1}, r_{d1}) \\ \vdots \\ \Phi(r_{sm}, r_{dm}) \end{pmatrix} = \begin{pmatrix} W_{11} & \dots & W_{1n} \\ \vdots & \ddots & \vdots \\ W_{m1} & \dots & W_{mn} \end{pmatrix} \times \begin{pmatrix} \delta\mu_a(r_1) \\ \vdots \\ \delta\mu_a(r_n) \end{pmatrix} \tag{1}$$

where $\Phi(r_{si}, r_{di})$ is the diffuse perturbative phase for the ith source–detector pair, W_{ij} (O'Leary 1996) is the weight for the jth voxel and the ith source–detector pair and $\delta\mu_a(r_j)$ is the differential absorption coefficient of the jth voxel. We limited our problem to image the absorption coefficient. Boundary conditions for semi-infinite geometries and slab geometries are derived using the extrapolated boundary condition and the image source technique (Haskell *et al* 1994).

2.2. Functional imaging

The estimation of the absorption coefficient at several wavelengths enables the provision of spatial maps of the targeted chromophores. In the case of the breast, the four chromophores of potential diagnostic interest are the oxy- and deoxy-haemoglobin, the water and the lipid.

The concentrations of these breast constituents are linearly related to the absorption values through the linear system:

$$\begin{pmatrix} \delta\mu_{\mathrm{a}}^{\lambda 1}(r_j) \\ \vdots \\ \delta\mu_{\mathrm{a}}^{\lambda p}(r_j) \end{pmatrix} = \begin{pmatrix} \varepsilon_{\mathrm{Hb}}^{\lambda 1} & \varepsilon_{\mathrm{HbO_2}}^{\lambda 1} & \varepsilon_{\mathrm{H_2O}}^{\lambda 1} & \varepsilon_{\mathrm{Li}}^{\lambda 1} \\ \vdots & \vdots & \vdots & \vdots \\ \varepsilon_{\mathrm{Hb}}^{\lambda p} & \varepsilon_{\mathrm{HbO_2}}^{\lambda p} & \varepsilon_{\mathrm{H_2O}}^{\lambda p} & \varepsilon_{\mathrm{Li}}^{\lambda p} \end{pmatrix} \times \begin{pmatrix} \delta[\mathrm{Hb}](r_j) \\ \delta[\mathrm{HbO_2}](r_j) \\ \delta[\mathrm{H_2O}](r_j) \\ \delta[\mathrm{Li}](r_j) \end{pmatrix} \tag{2}$$

where $\delta\mu_{\mathrm{a}}^{\lambda k}(r_j)$ is the differential absorption coefficient at the kth wavelength λ_k and for the jth voxel, $\varepsilon_C^{\lambda k}$ is the extinction coefficient of the Cth chromophore at the kth wavelength and $\delta[C](r_j)$ is the differential concentration of the Cth chromophore for the jth voxel.

Solving this linear system on a voxel basis for a spectral set of absorption distributions gives the functional maps required for diagnostic purposes. We will refer to this approach as 'indirect imaging' through this paper.

Recently, to overcome the burden and minimize the systematic errors due to the ill-condition of both inverse problems, a method aiming at directly imaging the functional parameters has been proposed (Durduran *et al* 2001). This method takes advantage of the linear relationship described previously and formulates the inverse problem as

$$\begin{pmatrix} \Phi^{\lambda 1}(r_{\mathrm{s}1}, r_{\mathrm{d}1}) \\ \vdots \\ \Phi^{\lambda 1}(r_{\mathrm{s}m}, r_{\mathrm{d}m}) \\ \vdots \\ \Phi^{\lambda p}(r_{\mathrm{s}1}, r_{\mathrm{d}1}) \\ \vdots \\ \Phi^{\lambda p}(r_{\mathrm{s}m}, r_{\mathrm{d}m}) \end{pmatrix} = \begin{pmatrix} \varepsilon_{\mathrm{Hb}}^{\lambda 1} W^{\lambda 1} & \varepsilon_{\mathrm{HbO_2}}^{\lambda 1} W^{\lambda 1} & \varepsilon_{\mathrm{H_2O}}^{\lambda 1} W^{\lambda 1} & \varepsilon_{\mathrm{Li}}^{\lambda 1} W^{\lambda 1} \\ \varepsilon_{\mathrm{Hb}}^{\lambda 2} W^{\lambda 2} & \varepsilon_{\mathrm{HbO_2}}^{\lambda 2} W^{\lambda 2} & \varepsilon_{\mathrm{H_2O}}^{\lambda 2} W^{\lambda 2} & \varepsilon_{\mathrm{Li}}^{\lambda 2} W^{\lambda 2} \\ \vdots & \vdots & \vdots & \vdots \\ \varepsilon_{\mathrm{Hb}}^{\lambda p} W^{\lambda p} & \varepsilon_{\mathrm{HbO_2}}^{\lambda p} W^{\lambda p} & \varepsilon_{\mathrm{H_2O}}^{\lambda p} W^{\lambda p} & \varepsilon_{\mathrm{Li}}^{\lambda p} W^{\lambda p} \end{pmatrix} \times \begin{pmatrix} \delta[\mathrm{Hb}](r_j) \\ \delta[\mathrm{HbO_2}](r_j) \\ \delta[\mathrm{H_2O}](r_j) \\ \delta[\mathrm{Li}](r_j) \end{pmatrix}. \tag{3}$$

This new linear system is poorly conditioned and great care should be taken during the pre-conditioning of this sensitivity matrix. In our case, we used an average column scheme (Pei *et al* 2001) applied to each sub-matrix of the kernel as written in (3). This specific pre-conditioning scheme led to the most accurate reconstructions. We will refer to the scheme expressed in (3) as 'direct imaging' through this document.

The functional parameters that we are interested in are the blood volume:

$$[\mathrm{BV}] = [\mathrm{Hb}] + [\mathrm{HbO_2}] \tag{4}$$

and the relative saturation:

$$[\mathrm{SaO_2}] = \frac{[\mathrm{HbO_2}]}{[\mathrm{Hb}] + [\mathrm{HbO_2}]}. \tag{5}$$

2.3. Bayesian framework

Due to the ill-posed and/or underdetermined nature of the DOT problem, the solution of the inverse problem is not typically robust. One avenue to overcome this difficulty is to incorporate *a priori* information constraining the space of unknowns.

The Bayesian approach provides a natural framework to incorporate prior information. Guven *et al* (2004) proposed an algorithm based on the Bayesian framework with a spatially varying *a priori* probability density function extracted from MRI anatomical maps. Here we propose to extend this algorithm to a spatial physiological prior. The full derivation of the theoretical developments for the algorithm is presented in detail in Guven *et al* (2004) and we

follow herein the same mathematical expressions. We present in this investigation only the salient features of the theoretical approach that are relevant to this work.

The available high-resolution anatomical image is segmented into sub-images that represent major tissue types (typically: parenchyma, glandular and tumour). Prior probability density function of the image is formulated in such a way that each sub-image is assigned a mean value that need not be equal to its actual optical value; and a 'confidence level' is defined in the form of an image variance formulation to allow local variations within sub-images. As a consequence, the overall formulation of the prior information becomes spatially varying, which is specific to the image of interest. Maximum *a posteriori* (MAP) estimate of the image is formed based on the formulation of the image's probability density function

$$\hat{x}_{\mathrm{MAP}} = \arg\max_{x}\{\log p(y|x) + \log p(x)\} \tag{6}$$

where $p(y|x)$ is the data likelihood function and $p(x)$ is the probability density function of the corresponding image. An 'alternating minimization' algorithm, which sequentially updates the unknown parameters, is used to solve the resulting optimization problem.

For our purposes, the probability density function of the ith sub-image, as defined in the spatial prior, becomes

$$p(\boldsymbol{x}_i|\sigma_i) = \frac{1}{\left(2\pi\sigma_i^2\right)^{N_i/2}} \exp\left(-\frac{1}{2\sigma_i^2}\|\boldsymbol{x}_i - \boldsymbol{C}_i\|^2\right) \qquad i = 1, 2, \ldots, M \tag{7}$$

where M is the number of sub-regions and N_i is the number of voxels in the ith sub-image, $\boldsymbol{x}_i$ is the unknown sub-image, $\boldsymbol{C}_i$ is the assigned chromophore mean concentration and σ_i^2 the single variance, which is an unknown parameter (estimated during the solution). To incorporate the confidence level into the statistical reconstruction procedure, the sub-image variances are expressed as

$$p(\sigma_i) = \frac{1}{\left(2\pi\gamma_i^2\right)^{N_i/2}} \exp\left(-\frac{1}{2\gamma_i^2}\|\sigma_i - \bar{\sigma}_i\|^2\right) \qquad i = 1, 2, \ldots, M \tag{8}$$

where γ_i is the variance and $\bar{\sigma}_i$ the mean value of σ_i. These two last parameters are *a priori* defined by the user. Thus the confidence level incorporated into the statistical reconstruction procedure is defined on the chromophores concentration. Hence, physiological priors are implicitly defined and allow constraining the reconstruction in physiologically meaningful ranges.

2.4. Measurement generation

Measurements were obtained by solving the frequency-domain diffusion equation with a finite difference approach (FDM). We restricted our simulations to a two-dimensional (2D) geometry for computational efficiency and to a continuous wave data set type. The slab thickness was 6 cm simulating a soft compressed breast. We placed nine sources on one side of the slab and nine detectors on the other side, both evenly stretched along 8 cm (cf figure 1). Two square inclusions of 1 cm^2 were simulated in this model.

The functional properties were chosen to mimic typical values encountered in the human breast. Table 1 summarizes the functional parameters simulated.

The optical models were computed for six wavelengths to replicate the spectral information gathered by our time resolved instrument that performs co-registration with MRI (Intes *et al* 2002). The subsequent optical properties are compiled in table 2. The FDM computations were performed with a 1 mm mesh resolution. The sources and detectors were positioned 2 cm away from the edges to avoid any boundary effects.

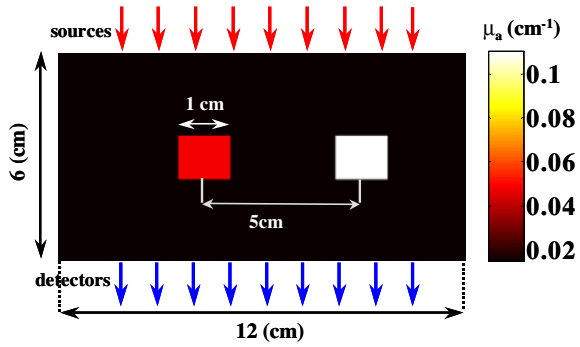

Figure 1. Optical model used for the simulations. The optical properties displayed here correspond to $\lambda = 750$ nm.

Table 1. Functional parameters used to define the optical properties to generate the synthetic measurements.

	Background	Left object	Right object
BV (mM)	0.02	0.06	0.12
SaO_2 (%)	70	65	50

Table 2. Optical parameters for the spectral set investigated herein. No [H_2O] and [Li] constituents were used in these simulations for simplicity.

	690	750	780	805	830	850
μ_s' (cm^{-1})	9.268	8.386	8.000	7.646	7.425	7.216
$\mu_a^{bkg.}$ (cm^{-1})	0.016	0.016	0.016	0.016	0.018	0.019
μ_a^{Left} (cm^{-1})	0.054	0.050	0.050	0.049	0.053	0.056
μ_a^{Right} (cm^{-1})	0.140	0.115	0.107	0.095	0.100	0.105

3. Results

First, the estimation of the functional parameters simulated is accomplished with a conjugate gradient descent (CGD) algorithm in the case of indirect imaging without using any kind of prior. The results are displayed in figure 2.

Then reconstructions using the indirect imaging approach within the Bayesian framework are provided in figure 3. First, an estimation of the absorption coefficients at the six wavelengths was performed using spatial *a priori* information and a conjugate gradient algorithm with the Polak–Ribiere method (Polak and Ribiere 1969). The absorption coefficients mean values assigned were the simulated ones with a 30% level of confidence (Guven *et al* 2004). Then classical spectroscopy was performed on the resulting optical maps using the linear system of (3) reduced to [HbO_2] and [Hb] concentrations. Last, the results using physiological and spatial *a priori* information are depicted in figure 4. The chromophore concentration means assigned were the exact ones with a 30% level of confidence.

The functional quantitative values retrieved from each case and for the relevant region of interest are summarized in table 3.

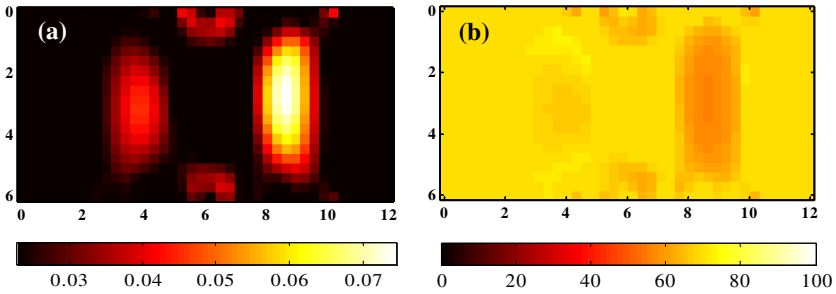

Figure 2. (a) Blood volume (mM) reconstructions and (b) saturation estimates (%) in the case of classical indirect imaging.

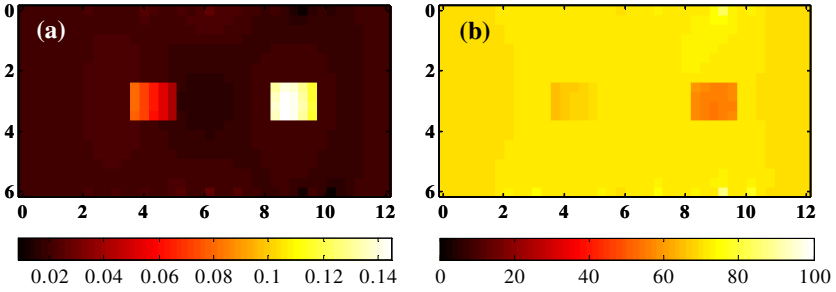

Figure 3. (a) Blood volume (mM) reconstructions and (b) saturation estimates (%) in the case of Bayesian indirect imaging. The assigned mean values of the absorption correspond to the true absorption values with a 30% level of confidence.

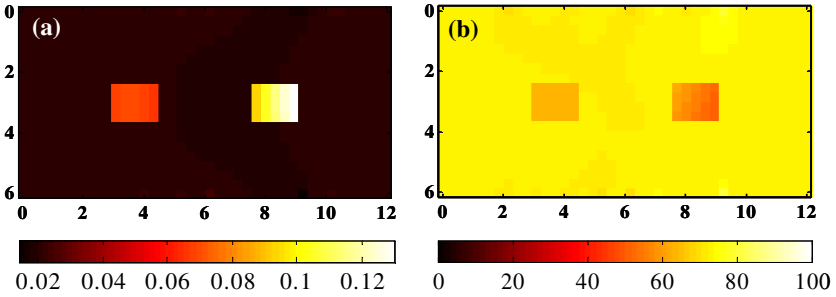

Figure 4. (a) Blood volume (mM) reconstructions and (b) saturation estimates (%) in the case of Bayesian direct imaging. The assigned mean values correspond to the true concentration values with a 30% level of confidence.

4. Discussion

In all the cases investigated herein, the two inclusions were reconstructed. As expected, the incorporation of spatial *a priori* information increased the image resolution. In the case of indirect imaging without *a priori* information the two inclusions are elongated and thus the contrast is diluted. This fact is reflected in the estimation of the blood volume that is underestimated for both objects (∼35% lower estimate). When *a priori* anatomical information is incorporated within the Bayesian framework, the estimation of the blood volume is more

Table 3. Functional parameters recovered with the three approaches and for the three different functional areas. The values proposed here correspond to the mean value of the entire ROI defined as the *a priori* spatial masks. [BV] in mM and [SaO_2] in %.

	Background		Left object		Right object	
	[BV]	[SaO_2]	[BV]	[SaO_2]	[BV]	[SaO_2]
Indirect imaging	0.023	71	0.042	67	0.075	57
Bayesian indirect imaging	0.019	72.46	0.065	63.73	0.122	55.44
Bayesian direct imaging	0.020	69.95	0.061	65.27	0.127	50.02

accurate falling to less than 10% of misestimation in the worse case (1% in the best case). Moreover, when direct imaging is applied in this framework, the two objects are recovered respectively within 1% and 5% for the left and right objects compared to 8% and 2% in the case of indirect imaging.

The enhancement of the technique is even more notable when SaO_2 is considered. The recovery of SaO_2 is then more robust but also less prone to artefacts. Especially in the case of the right object, the recovery of the SaO_2 is superior to the direct imaging approach within the Bayesian framework.

Overall, these simulations highlight the potential of our approach to provide more accurate maps of the relevant functional diagnostic parameters. These simulations were limited to [BV] and SaO_2 recovery. The approach is easily extensible to [H_2O] and [Li]. Especially, the ability of MRI to provide spatial concentration of these chromophores for the assigned prior strengthens our approach (Merrit *et al* 2003).

The mean values of the chromophores and the anatomical *a priori* information are defined by the user. The anatomical maps are provided by the structural MRI maps (such as T1) and tumour delineation could be performed by Gd enhanced MRI. Moreover, estimation of the water, lipid and BV concentrations are feasible with MRI. These values can be used for the mean concentration priors. Also, an alternative is to obtain these values with a simple algorithm such as diffuse optical spectroscopy (Ntziachristos *et al* 2002). The paradigm of uniform concentrations for a certain tissue type is overcome in the Bayesian formulation by defining a level of confidence. These effects of confidence ensure the reconstructions are in a physiologically meaningful range and allow the recovery of heterogeneous concentration in a certain kind of tissue type. Such heterogeneous estimates are visible in figures 3 and 4.

This last point is of paramount importance in the case of MRI-assisted DOT. The contrast provided by MRI is not expected to be exactly congruent with the optical contrast. Allowing heterogeneous bounded reconstructions within each sub-image compensates for discrepancies between both modalities.

5. Conclusion

We reported in this work our first step towards incorporating physiological and spatial *a priori* information derived from MRI to assist DOT. Better estimates of the main functional parameters that are [BV] and [SaO_2] were achieved. More accurate functional maps can lead to an increase of the sensitivity and specificity of optical techniques by incorporating structural contrasts that are known to occur in breast cancer. Moreover, these accurate estimations will be important for application such as therapy monitoring (Zhang *et al* 2003).

This preliminary work will be continued with experimental validation and incorporated in our ongoing clinical trial at the University of Pennsylvania. Also, the investigation will be

extended to the potential of our approach to recover exogenous contrast agent concentrations. New classes of contrast agents that are tumour specific (Licha 2002) and/or compatible with both technologies (Josephon *et al* 2002) will be investigated. The inclusion of spatial and temporal *a priori* information is expected to provide a better estimate of the fluorochrome concentration but also to probe physiological parameters such as extravasation (Intes *et al* 2003, Cuccia *et al* 2003) that are still elusive with DOT for thick tissue investigation.

Acknowledgments

XI and BC acknowledge partial support from the National Institute of Health grant no CA 87046.

References

Arridge S 1999 Optical tomography in medical imaging *Inverse Problems* **15** R41–R93

Brooksby B, Dehghani H, Pogue B and Paulsen K 2003 Near-infrared tomography breast image reconstruction with *a priori* structural information from MRI: algorithm development for reconstructing heterogeneities *IEEE J. Sel. Top. Quantum Electron.* **9** 199–209

Cerussi A, Berger A, Bevilacqua F, Shah N, Jakubowski D, Butler J, Holcombe R and Tromberg B 2001 Sources of absorption and scattering contrast for near-infrared optical mammography *Acad. Radiol.* **8** 211–8

Cerussi A and Tromberg B 2003 Optical mammography inches closer to the clinics *Biophotonics* 38–42

Chance B 2001 Near-infrared optical spectroscopy characterizes breast tissue hormonal and age status *Acad. Radiol.* **8** 209–10

Colak S, van der Mark M, Hooft G, Hoogenraad J, van der Linden E and Kuijpers F 1999 Clinical optical tomography and NIR spectroscopy for breast cancer detection *IEEE J. Sel. Top. Quantum Electron.* **5** 1143–58

Cubeddu R, D'Andrea C, Pifferi A, Taroni P, Torricelli A and Valentini G 2000 Effects of the menstrual cycle on the red and near-infrared optical properties of the human breast *Photochem. Photobiol.* **72–73** 383–91

Cuccia D, Bevilacqua F, Durkin A, Merritt S, Tromberg B, Gulsen G, Yu H, Wang J and Nalcioglu O 2003 *In vivo* quantification of optical contrast agent dynamics in rat tumors by use of diffuse optical spectroscopy with magnetic resonance imaging coregistration *Appl. Opt.* **42** 2940–50

Durduran T, Choe R, Culver J, Zubkov L, Holboke M, Giammarco J, Chance B and Yodh A G 2002 Bulk optical properties of healthy female breast tissue *Phys. Med. Biol.* **47** 2847–61

Durduran T, Giammarco J, Culver J, Choe R, Zubkov L, Holboke M, Intes X, Nioka S, Chance B and Yodh A 2001 Utilizing *a priori* spectral knowledge in diffuse optical tomography *United Engineering Foundation Conf. Advances in Optics for Biotechnology, Medicine and Surgery VII*

Franceschini M, Moesta K, Fantini S, Gaida G, Gratton E, Jess H, Mantulin W, Seeber M, Schlag P and Kaschke M 1997 Frequency-domain techniques enhance optical mammography: initial clinical results *Proc. Natl Acad. Sci. USA* 6468–73

Grosenick D, Moesta T, Wabnitz H, Mucke J, Stroszcynski C, Macdonald R, Schlag P and Rinnerberg H 2003 Time-domain optical mammography: initial clinical results on detection and characterization of breast tumors *Appl. Opt.* **42** 3170–86

Guven M, Yazici B, Intes X, Maloux C and Chance B 2004 Three-dimensional diffuse optical tomography with *a priori* anatomical information *J. Biomed. Opt.* submitted

Haskell R, Svaasand L, Tsay T T, Feng Tc, McAdams M and Tromberg B 1994 Boundary conditions for the diffusion equation in radiative transfer *J. Opt. Soc. Am.* A **11** 2727–41

Intes X, Yu J, Yodh A G and Chance B 2002 Development and evaluation of a multi-wavelength multi-channel time resolved optical instrument for NIR/MRI mammography co-registration *Proc. IEEE 28th Annual Northeast Bioengineering Conf. (IEEE Cat. No.02CH37342)* pp 91–2

Intes X, Ripoll J, Chen Y, Nioka S, Yodh A and Chance B 2003 *In vivo* continuous-wave optical breast imaging enhanced with Indocyanine Green *Med. Phys.* **30** 1039–47

Jiang H, Iftimia N, Eggert J, Fajardo L and Klove K 2002 Near-infrared optical imaging of the breast with model-based reconstruction *Acad. Radiol.* **9** 186–94

Josephon L, Kircher M, Mahmood U, Tang Y and Weissleder R 2002 NIR fluorescent nanoparticles as combined MR/optical imaging probes *Bioconjug. Chem.* **13** 554–60

Licha K 2002 Contrast agents for optical imaging *Top. Curr. Chem.* **222** 1–29

Lin Y, Lech G, Nioka S, Intes X and Chance B 2002 Noninvasive, low-noise, fast imaging of blood volume and deoxygenation changes in muscles using light-emitting diode continuous-wave imager *Rev. Sci. Instrum.* **73** 3065–74

McBride T, Pogue B, Jiang S, Osterberg U and Paulsen K 2001 Initial studies of *in-vivo* absorbing and scattering heterogeneity in near-infrared tomographic breast imaging *Opt. Lett.* **26** 822–4

Merritt S, Gulsen G, Chiou G, Chu Y, Deng C, Cerussi A, Durkin A, Tromberg B and Nalcioglu O 2003 Comparison of water and lipid content measurements using diffuse optical spectroscopy and MRI in emulsion phantoms *Technol. Cancer Res. Treat.* **2** 563–9

Ntziachristos V, Yodh A, Schnall M and Chance B 2002 MRI-guided diffuse optical spectroscopy of malignant and benign breast legions *Neoplasia* **4** 347–54

O'Leary M 1996 Imaging with diffuse photon density waves *PhD Thesis* University of Pennsylvania

Pei Y, Bao F and Barbour R 1999 Modeling of sensitivity and resolution to an included object in homogeneous scattering media and in MRI-derived breast maps *Opt. Exp.* **5** 203–19

Pei Y, Graber H and Barbour R 2001 Normalized constraint algorithm for minimizing inter-parameter crosstalk in DC optical tomography *Opt. Exp.* **9** 97–109

Pogue B and Paulsen K 1998 High-resolution near-infrared tomographic imaging simulations of the rat cranium by use of *a priori* magnetic resonance imaging structural information *Opt. Lett.* **23** 1716–8

Polak E and Ribiere G 1969 Note sur la convergence de directions conjuguees *Rev. Fr. Inform. Rech. O.* **16** 35–43

Shah N, Cerussi A, Eker B, Espinoza J, Butler J, Fiskhin J, Hornung R and Tromberg B 2001 Non-invasive functional optical spectroscopy of human breast tissue *Proc. Natl Acad. Sci. USA* **98** 4420–5

Srinivasan S, Pogue B, Jiang S, Dehghani H, Kogel C, Soho S, Gibson J, Tosteson T, Poplack S and Paulsen K 2003 Interpreting hemoglobin and water concentration, oxygen saturation, and scattering measured *in vivo* by near-infrared breast tomography *Proc. Natl Acad. Sci. USA* **100** 12349–54

Strangman G, Boas D and Sutton J 2002 Non-invasive neuroimaging using near-infrared light *Biol. Psychiatry* **52** 679–93

Tromberg B, Shah N, Lanning R, Cerussi A, Espinoza J, Pham T, Svaasand L and Butler J 2000 Non-invasive *in vivo* characterization of breast tumors using photon migration spectroscopy *Neoplasia* **2** 26–40

Villringer A and Chance B 1997 Non-invasive optical spectroscopy and imaging of human brain function *Trends Neurosci.* **20** 435–42

Zhang J, Tu T, Sunar U, Intes X, Nioka S, Zhang Z, Kilger A, Lustig R, Loevner L and Chance B 2003 Application of I&Q detection system in scouting the curative effect of neck squamous cell carcinoma *Proc. SPIE Optical Tomography and Spectroscopy of Tissue V* **4955** 575–80